Available online at www.sciencedirect.com
ScienceDirect
International Journal of Mass Spectrometry 267 (2007) 43–53
International Journal of Mass Spectrometry
www.elsevier.com/locate/ijms

Protonation of heterocyclic aromatic molecules: IR signature of the protonation site of furan and pyrrole

Ulrich Joseph Lorenz [a], Joel Lemaire [b], Philippe Maitre [b], Maria-Elisa Crestoni [c], Simonetta Fornarini [c], Otto Dopfer [a,*]

[a] *Institut für Optik und Atomare Physik, Technische Universität Berlin, Hardenbergstrasse 36, D-10623 Berlin, Germany*
[b] *Laboratoire de Chimie Physique, UMR8000 CNRS-Université Paris-Sud 11, Faculte des Sciences d' Orsay, Bâtiment 350, F-91405 Orsay Cedex, France*
[c] *Dipartimento di Studi di Chimica e Tecnologia delle Sostanze Biologicamente Attive, Università di Roma La Sapienza, Piazzale A. Moro 5, I-00185 Roma, Italy*

Received 1 September 2006; received in revised form 27 January 2007; accepted 20 February 2007
Available online 23 February 2007

Abstract

Protonated furan ($C_4H_5O^+$, furanH$^+$) and protonated pyrrole ($C_4H_6N^+$, pyrroleH$^+$) are generated by chemical ionization of the respective parent molecules in the cell of an FT-ICR mass spectrometer using $CH_5^+/C_2H_5^+$ as protonating agents. The protonation site is investigated by resonant infrared multiphoton dissociation (IRMPD) spectroscopy in the 900–1700 cm^{-1} fingerprint range employing the free electron laser (FEL) at the Centre Laser Infrarouge Orsay (CLIO). Comparison with quantum chemical calculations at the B3LYP/6-311G(2df, 2pd) level of theory demonstrates unambiguously that only the C_α protonated isomers are observed, which correspond to the global minima on the potential energy surfaces of both protonated heterocyclic molecules. Spectroscopic features corresponding to protonation at the C_β atom or at the heteroatom are not detected. The IRMPD spectra correspond to the first spectroscopic identification of both protonated heterocyclic molecules in the gas phase. During the course of the experiments, the IRMPD spectrum of the furan radical cation ($C_4H_4O^+$, furan$^+$) has been detected as well. Comparison of the IR spectra of the neutral molecules with the IRMPD spectra of the radical cation and the protonated species reveals the effects of both ionization and protonation on the structural properties of these fundamental heterocyclic molecules.

Keywords: IR spectroscopy; Structure elucidation; Protonated aromatic heterocycle; Reactive intermediate; Carbocation

1. Introduction

Proton transfer constitutes one of the most elementary chemical reactions, with the proton being the conceivably most simple reagent [1]. Protonation steps and protonation equilibria play a crucial role in a variety of organic reaction mechanisms, ranging from simple ester hydrolysis to complex metal organic reactions, as well as in biomolecular processes, such as protein folding and acid-catalyzed enzymatic reactions [2,3].

In addition, protonation is one of the major ionization techniques in mass spectrometry and thereby represents the most simple gas phase reaction that can be realized in a mass spectrometer. The relevance for solution phase chemistry, the possibility to study protonation in a solvent free environment with clearly defined protonating agents and unsolvated products, and the opportunity to use potent protonating agents for the generation of high-energy species that would possess short lifetimes in solution has lead to numerous studies, in which gas phase basicities and proton affinities have been determined. An exhaustive and frequently used compilation of these fundamental thermodynamic quantities has been provided by Hunter and Lias [4].

Although thermodynamic and kinetic properties of protonation and deprotonation processes are readily accessible for many molecules by mass spectrometric studies, structural information is often more difficult to obtain and is in some cases ambiguous [5]. An interesting problem arises for molecules with different competing protonation sites, as in the case of the simple heterocyclic molecules investigated in the present work. These include furan and pyrrole, for which protonation can occur at

* Corresponding author. Tel.: +49 30 314 23017; fax: +49 30 314 23018.
E-mail address: dopfer@physik.tu-berlin.de (O. Dopfer).

1387-3806/$ – see front matter © 2007 Elsevier B.V. All rights reserved.
doi:10.1016/j.ijms.2007.02.017

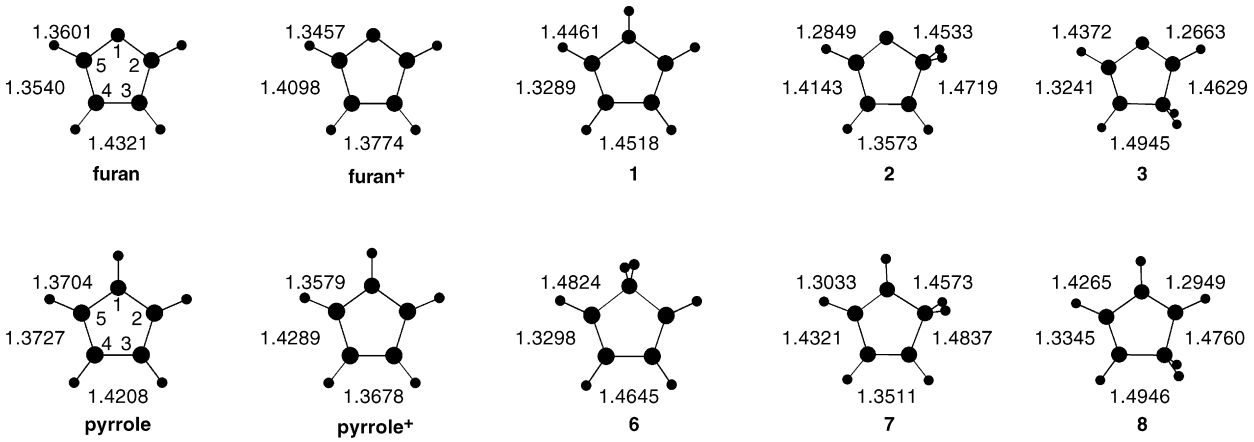

Fig. 1. Structures of furan and pyrrole, their radical cations, and their protonated molecules evaluated at the B3LYP/6-311G(2df, 2pd) level of theory. C–X bond lengths (X = C, O, N) are listed in Å to illustrate the influence of ionization and protonation on the geometry of the aromatic ring.

the heteroatom or at one of the two nonequivalent carbon atoms (Fig. 1). Proton exchange in these heterocyclic molecules can be considered as a fundamental example of the electrophilic aromatic substitution mechanism, with the proton being the electrophile [2]. This reaction is known to proceed in the condensed phase through a high-energy intermediate, namely the so-called σ complex (Wheland intermediate), in which the entering electrophile forms a chemical bond to one of the ring carbon atoms, with the concurrent loss of aromaticity [2,6,7]. Five-membered aromatic heterocycles and their derivatives are also interesting biomolecular building blocks [3,8,9] and play an important role in organic synthesis [10,11], polymer chemistry, and material science [12–14].

The challenge of characterizing protonated heterocyclic molecules in the condensed phase has been addressed in NMR spectroscopic studies, which generally agree that the C_α protonated species of furanH^+ (**2**) and pyrroleH^+ (**7**) correspond to the most stable isomers [2,11,15]. For pyrroleH^+, although C_α protonation is thermodynamically favored, kinetic NMR studies also reveal protonation at both N and C_β, with the relative reaction rates for proton exchange strongly depending on the solvent [16–18]. In the gas phase, both C_α and C_β protonation has indirectly been evidenced from isotopic labeling and reactivity studies, with the ratio of both isomers strongly depending on the experimental conditions [19–22]. Quantum chemical calculations demonstrate that the C_α protonated species corresponds to the global minimum of the potential energy surface, whereas the C_β and O/N protonated isomers are higher-energy local minima [22–27].

The aim of the present study is to gather for the first time spectroscopic information for furanH^+ and pyrroleH^+ in the gas phase by means of IR spectroscopy, in order to provide unambiguous information about the protonation site(s) observed under isolated conditions. Two major IR spectroscopic strategies have recently been developed to address the question of the structure and energetics of protonated aromatic molecules (AH^+) by direct comparison of experimental IR spectra with those calculated by quantum chemical techniques. Both successful approaches rely on infrared photodissociation (IRPD) schemes performed in tandem mass spectrometers and details of their application to (microsolvated) protonated aromatic molecules are described in a recent review [28]. Briefly, the first methodolgy involves single photon IRPD spectroscopy of either isolated AH^+ ions or microsolvated AH^+–L_n cluster ions (L = ligand) in a tandem quadrupole mass spectrometer using optical parametric oscillator laser systems in the 2500–4000 cm^{-1} range, in order to probe the X–H stretch vibrations (X = C, N, O, F). Applications include the characterization of $AH^+(–L_n)$ with A = benzene [29–31], fluorobenzene [32,33], (*para*-halogenated) phenols [34–38], aniline [39], imidazole [40], and pyridine [31]. The second approach utilizes IR multiphoton dissociation (IRMPD) spectroscopy in a Fourier transform ion cyclotron resonance (FT-ICR) mass spectrometer or a quadrupole ion trap using high-intensity free electron lasers (FEL) in the complementary 500–2500 cm^{-1} fingerprint range [41,42]. The AH^+ ions investigated with this technique include A = benzene [41], fluorobenzene [43], toluene [44,45], indazole [46], phenylsilane [47], benzaldehyde [48], and benzoic acid [49]. The present work applies IRMPD spectroscopy to obtain the first spectroscopic data of isolated furanH^+ ($C_4H_5O^+$) and pyrroleH^+ ($C_4H_6N^+$). In fruitful combination with quantum chemical calculations, the observed IRMPD spectra are unambiguously assigned to the C_α protonated isomers. During the course of the experiments, the IRMPD spectrum of the furan radical cation ($C_4H_4O^+$) has been detected as well. Comparison of the IR spectra of the neutral molecules with the IRMPD spectra of the radical cation and the protonated species unravels the effects of both ionization and protonation on the structural properties of these fundamental heterocyclic molecules.

2. Experimental and computational methods

IRMPD spectra of mass-selected ions are recorded in a mobile FT-ICR mass spectrometer analyzer (MICRA) using tuneable IR radiation provided by the FEL at CLIO. Details of the coupling of MICRA [50] with the FEL [51] have been described previously. Briefly, furanH^+ and pyrroleH^+ are produced in the ICR cell by chemical ionization of the parent molecules using methane. For this purpose, a 50 ms pulse of gaseous furan or pyrrole at pressures of $1–4 \times 10^{-6}$ mbar is

injected into the FT-ICR cell together with a 200 ms pulse of CH_4 (10^{-6} mbar). The mixture is then ionized by a 100 ms electron pulse (70 eV) and left for 600 ms to equilibrate. Previous experiments for the reaction of protonated furan with acetone carried out under similar FT-ICR conditions suggest that this reaction time should be sufficient to reach equilibrium for comparable proton transfer reactions [23]. Mass spectra recorded 100 ms after the electron pulse indicate that $C_2H_5^+$ is by far the predominant protonating agent, although contributions of fast reacting CH_5^+ cannot be ruled out. The species of interest is mass-selected and then irradiated with FEL radiation for 5–10 s, which corresponds to a significantly longer irradiation time (roughly one order of magnitude) compared to most previous studies using the same experimental setup [43,44,47,48,52]. In an attempt to record simultaneously the IRMPD spectra of both the radical cations and the protonated species, i.e., furan(H)$^+$ or pyrrole(H)$^+$, both species are mass-selected in this step. There is no interference in their IRMPD spectra because the photodissociation channels of the two parent species are different (*vide infra*). A similar strategy has recently been applied to obtain the IRMPD spectra of indazole(H)$^+$ and benzoic acid(H)$^+$ [46,49]. The FEL radiation is composed of 8 μs macropulses (25 Hz), each divided into 500 micropulses with a spacing of 16 ns and a width of a few ps. The mean power of typically 1 W corresponds to micropulse and macropulse energies of 80 μJ and 40 mJ, respectively, and to a peak power of the order of 80 MW. The FEL is operated at 45 MeV providing radiation in the 900–1700 cm^{-1} spectral range, with a typical bandwidth of 0.5% for the central wavelength. After irradiation, mass spectra are recorded at each wavelength of the IR laser in order to monitor parent and fragment ions. For each wavelength, the mass spectrum is obtained as the Fourier transform of the signals accumulated over five sequences. The IRMPD efficiency is evaluated as $R = -\ln[I_{\text{parent}}/(I_{\text{parent}} + I_{\text{fragments}})]$. The R values are not corrected for laser intensity variations. However, the spectral dependence of the laser power as a function of the laser frequency is shown along with the experimental IRMPD spectra. For further details of the IRMPD technique along with some theoretical considerations of the process, the reader is referred to a recent review article [42].

Quantum chemical calculations are performed for furanH$^+$ and pyrroleH$^+$ at the B3LYP/6-311G(2df, 2pd) level of theory in order to evaluate their potential energy surfaces (PES) [53]. Previous calculations revealed that this theoretical level reliably describes the PES of protonated aromatic molecules, with an accuracy similar to the MP2/6-311G(2df, 2pd) level [32,35]. Particular attention is paid to molecular structures, relative energies, and IR spectra of relevant potential minima, as well as feasible paths for isomerization and fragmentation. For comparison, additional calculations are carried out at the same theoretical level for the corresponding neutral molecules and their radical cations. All energies of stationary points are corrected for zero-point energies determined from harmonic vibrational wave numbers. For comparison with experimental IRMPD spectra, calculated harmonic vibrational wave numbers are scaled by a factor of 0.979 to account for anharmonicity. This scaling factor is derived from optimizing the agreement between experimental [54] and calculated frequencies of neutral furan and pyrrole in the 900–1800 cm^{-1} range.

3. Results and discussion

3.1. IRMPD spectra

Fig. 2 reproduces the IRMPD signals recorded for furanH$^+$, pyrroleH$^+$, and furan$^+$. The IRMPD signals of furanH$^+$ ($m = 69$ u) and pyrroleH$^+$ ($m = 68$ u) are exclusively observed in a single fragment channel, corresponding to elimination of CO ($m = 41$ u) and [HNC] ($m = 41$ u), respectively. In contrast, IRMPD signals of the furan radical cation ($m = 68$ u) are detected in three different fragment channels, corresponding to loss of CO ($m = 40$ u), C_2H_2 ($m = 42$ u), and [HCO] ($m = 39$ u), with integrated branching ratios of 92:5:3. In general, there is a good correspondence between the signal depletion observed in the parent ion channel and the appearance signals detected in the respective fragment ion channel(s). In addition, the positions of the peaks in the IRMPD signals of furanH$^+$ and furan$^+$ are different, indicating that there is no interference between the IRMPD

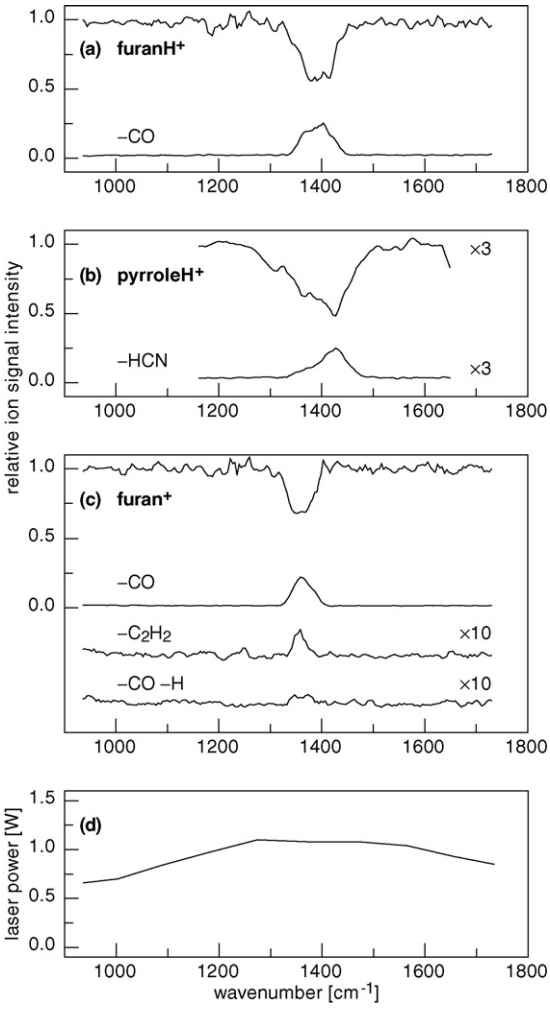

Fig. 2. IRMPD signals of furanH$^+$ (a), pyrroleH$^+$ (b), and furan$^+$ (c) recorded in various fragment channels. The laser power as a function of the IR wave number is shown in (d).

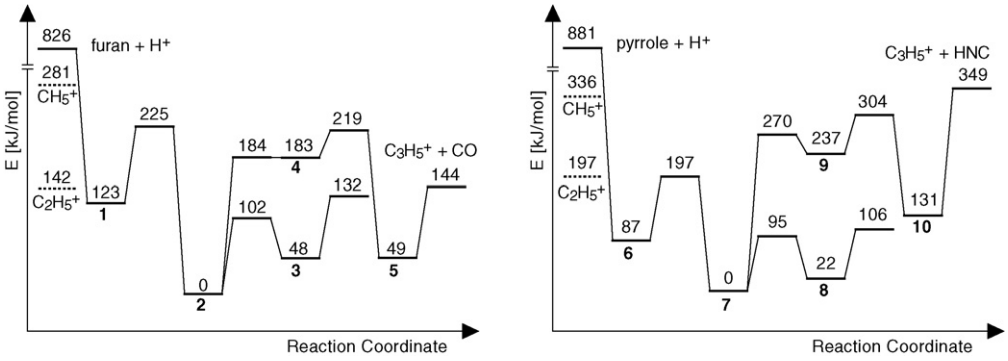

Fig. 3. Schematic potential energy surfaces of protonated furan and protonated pyrrole evaluated at the B3LYP/6-311G(2df, 2pd) level of theory. The dashed lines indicate the excess energies for protonation with CH_5^+ and $C_2H_5^+$. More details about the stationary points are given in the supplementary material.

spectra of both species, although they are recorded simultaneously. In addition to the IRMPD signals, Fig. 2 displays the laser power as a function of the IR wave number. The transitions observed in the IRMPD spectra have a typical width of the order of 50 cm^{-1}, although the widths of single transitions are as narrow as 30 cm^{-1} after peak deconvolution of partially overlapping vibrational absorptions.

Efforts in recording an IRMPD spectrum of the pyrrole radical cation have failed, probably due to the low IRMPD efficiency arising from inefficient intramolecular energy redistribution and/or its high dissociation energy. Similarly, efforts in recording IRMPD spectra of imidazoleH^+ and pyridineH^+ have been unsuccessful, despite the relatively long irradiation times of 5–10 s.

3.2. *FuranH^+*

Furan is a planar heterocyclic aromatic molecule (C_{2v}) offering three distinguishable protonation sites. Protonation can occur at the C_α and C_β atoms (**2**, **3**) as well as at the O atom (**1**). Their structures obtained at the B3LYP/6-311G(2df, 2pd) level are shown in Fig. 1. Their relative energies as well as other parts of the PES of furanH^+ relevant for isomerization and fragmentation processes are displayed in Fig. 3. In contrast to the three σ complexes (1–3), stable π complexes of a proton and furan could not be located as minima on the PES [29,55]. In agreement with previous theoretical studies [23–27], the relative energies of the complexes increase in the order **2** < **3** < **1** (0 < 48 < 123 kJ/mol). The derived proton affinities of 826, 778, and 703 kJ/mol for C_α, C_β, and O protonation are in reasonable agreement with recent values derived at the G3 level (815, 771, and 699 kJ/mol) [23], demonstrating that the B3LYP/6-311G(2df, 2pd) level chosen in the present work reliably describes the properties of these heterocyclic species. The proton affinity calculated for protonation at C_α, 826 kJ/mol, is in fair agreement with the experimental value of 812 kJ/mol determined by FT-ICR mass spectrometry [19,20,23], which is somewhat higher than the recommended and tabulated value obtained from high pressure mass spectrometry (803 kJ/mol) [4]. The calculated difference in the proton affinities for C_α and C_β protonation, 48 kJ/mol, is somewhat larger than the experimental estimate, 16 ± 5 kJ/mol [20]. The barriers for interconversion between the three minimum structures are larger than 50 kJ/mol, suggesting that, in principle, they could all be produced in noticeable abundances in suitable ion sources [32,35]. The PES in Fig. 3 also shows that protonation of furan is energetically feasible at all three protonation sites using CH_5^+ and/or $C_2H_5^+$ as protonating agent. In the condensed phase, protonation of furan occurs predominantly in C_α position, which is particularly relevant in electrophilic substitution reactions [2]. In the gas phase, mass spectrometric studies have demonstrated preferred protonation at the C_α position [19,20]. Interestingly, preferentially C_β protonation of furan was observed in a radiolytic study using very exothermic protonation with $^3He^3H^+$ and rationalized by kinetic rather than thermodynamic arguments [21].

Comparison of the structural parameters of furan and the various furanH^+ isomers (Fig. 1) demonstrates the massive effects of protonation on the geometry of the heterocyclic molecule, which drastically depend on the protonation site [24,26,27]. Significantly, protonation destroys the aromaticity of the six available π electrons, in particular for the C protonated species. The effects most relevant for the present work are the protonation-induced changes in the C–C and C–O bond lengths. For example, C_α protonation (at C_2) induces large elongations of the C_2–O, C_2–C_3, and C_4–C_5 bonds, and corresponding contractions of the C_3–C_4 and C_5–O bonds. These structural changes translate directly into modifications of the force constants of the associated vibrational coordinates, and thus lead to clearly different IR spectra predicted for the various furanH^+ isomers. Fig. 4 compares the linear IR absorption spectra calculated for the three favorable furanH^+ isomers in the fingerprint range of the skeletal ring stretching and bending modes (900–1800 cm^{-1}). Inspection of Fig. 4 reveals that the IR spectra of all three isomers are very different in this spectral range, indicating that IR spectroscopy provides an unambiguous diagnostic tool to distinguish between them. Comparison with the measured IRMPD spectrum in Fig. 4 leads to the straightforward conclusion that the carrier of the band observed in the experimental spectrum is clearly the most stable C_α protonated furanH^+ isomer (**2**). No spectral signatures of the other two isomers are visible in the experimental spectrum. The IRMPD spectrum displays a single band with a maximum at 1398 cm^{-1}, a total width of 65 cm^{-1}, and a depletion of the parent ion signal of the order of 45%. Deconvolution of the feature in two partly resolved bands assuming

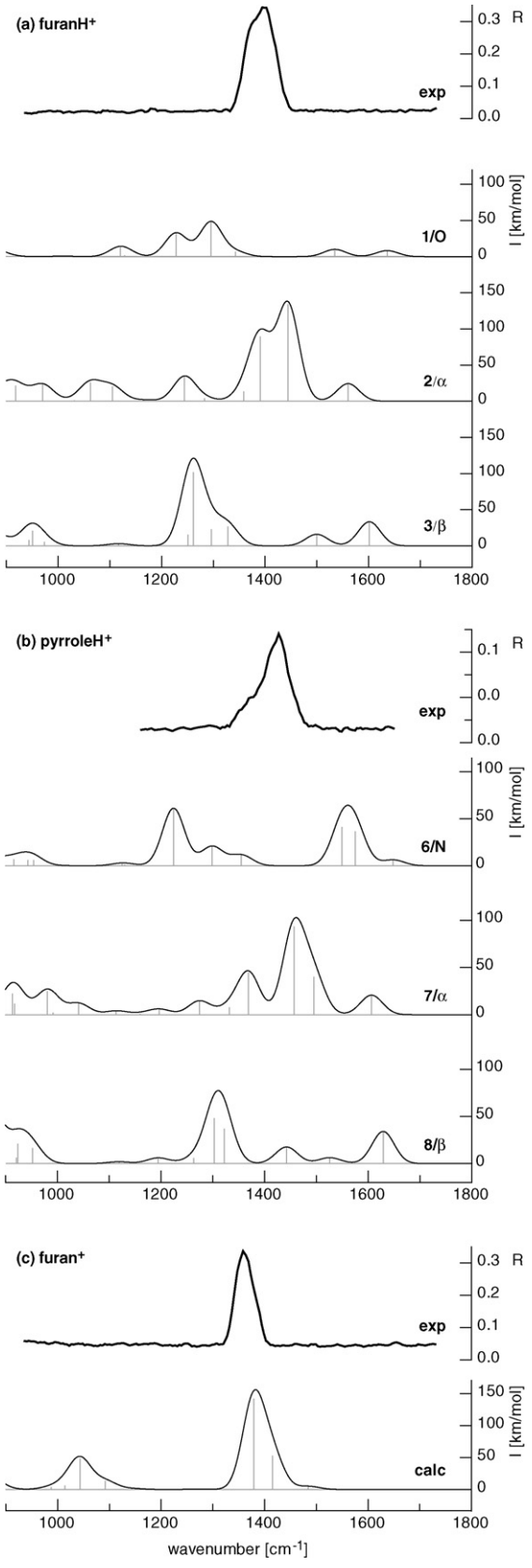

Fig. 4. Comparison of experimental IRMPD spectra (R) of furanH$^+$ (a), pyrroleH$^+$ (b), and furan$^+$ (c) to linear IR absorption spectra (km/mol) of possible isomers calculated at the B3LYP/6-311G(2df, 2pd) level of theory (scaling factor of 0.979, convolution width of 50 cm^{-1}).

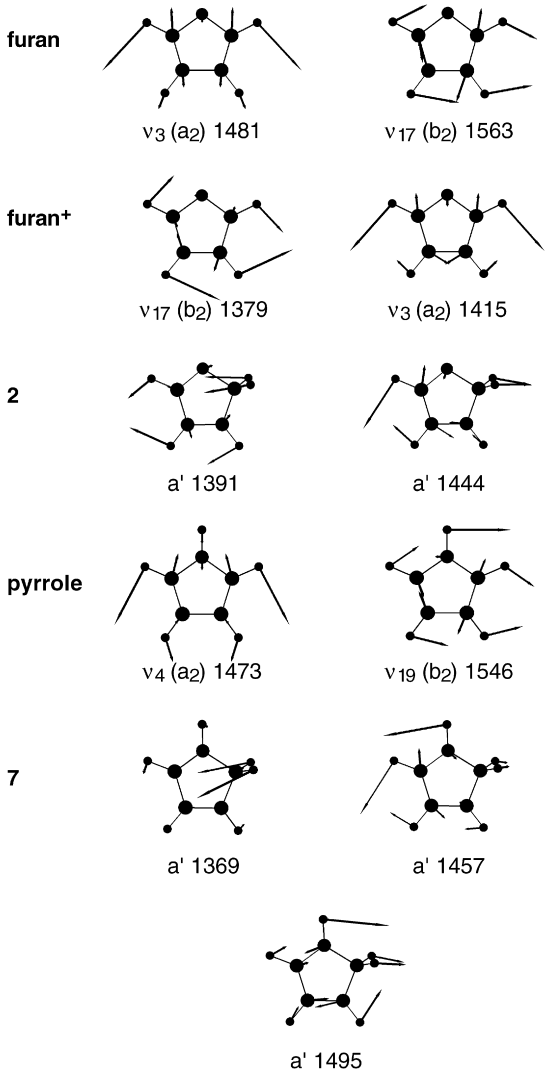

Fig. 5. Selected normal coordinates of furan$^{(+)}$, pyrrole, furanH$^+$ (**2**), and pyrroleH$^+$ (**7**) along with symmetries and scaled wave numbers.

Gaussian line shapes and using a convolution width of 39 cm^{-1} results in two components centered at 1374 and 1407 cm^{-1} with relative weights of 1:1.15. These contributions can readily be assigned to the two unresolved overlapping fundamentals of **2** predicted to occur at 1391 cm^{-1} (89 km/mol) and 1444 cm^{-1} (134 km/mol). The 1444 cm^{-1} mode corresponds mainly to a stretching motion of the C_4–C_5 bond, whereas the 1391 cm^{-1} mode is best described as a scissoring motion of the two H atoms of the aliphatic CH_2 group (Fig. 5). The asymmetric band profile observed in the experimental spectrum is consistent with the two predicted close-lying fundamentals featuring similar IR intensity. Other peaks occurring in the linear IR absorption spectrum of **2** are not present in the IRMPD spectrum, probably because their IR oscillator strengths (<40 km/mol) are below the critical threshold for efficient IRMPD (I_{th}, ~50 km/mol). The suppression of weakly IR-active modes in IRMPD spectra recorded with the same experimental setup has previously been reported for a variety of molecular ions with similarly high fragmentation thresholds [41,43]. Systematic studies for strongly bound systems, such as $Fe(CH_3OCH_3)_2^+$ [51], demonstrated that the

relative intensities of the IRMPD signals can strongly vary with the laser power and the IR oscillator strengths of the considered vibrational resonances. Another important factor influencing the IRPMD efficiency of a particular vibrational mode is the rate of intramolecular vibrational energy redistribution (IVR), which is an essential requirement for the IRMPD process to occur [42]. It is thus conceivable that for small molecular ions with high dissociation thresholds and low IVR rates after absorption of the first few IR photons, the IRMPD efficiency may converge to zero for weakly IR-active modes with intensities below a critical threshold I_{th} (typically of the order of 50 km/mol), even for the largest IR laser power available (∼1 W) and the relatively long irradiation time applied in the present work (up to 10 s). As a consequence, it is possible that any O protonated species of furanH$^+$ (1) may have escaped IRMPD detection, because the most intense transitions have calculated IR intensities of less than 50 km/mol in the considered spectral range, whereas the C_β protonated furanH$^+$ isomer (**3**), which features a sufficiently intense band at 1261 cm^{-1} (102 km/mol) to be detected by IRMPD, is clearly absent in the experimental spectrum.

The exclusive observation of C_α protonated furanH$^+$ (**2**) in the IRMPD spectrum may be rationalized by exothermic proton transfer reactions of the higher-energy furanH$^+$ isomers **1** and **3** with neutral furan molecules. As the gas mixture in the ICR cell has not been irradiated for 600 ms after the chemical ionization process, it can be assumed that by the time of the IRMPD measurement a thermodynamic equilibrium between the different furanH$^+$ isomers has been established through collisions between protonated and neutral furan molecules [23]. According to the calculated proton affinities of **1**–**3** and an effective temperature of the order of 350–400 K in the ICR cell [56], any initially produced isomers **1** and **3** will be converted into **2** [23,43]. In fact, the proton affinity of furan, as determined in similar ICR experiments, agrees well with the proton affinity calculated for C_α protonation, confirming that in ICR experiments only the most stable furanH$^+$ isomer is present after equilibration [23].

In a next step, possible photodissociation mechanisms of furanH$^+$ are considered. Interestingly, the dissociation pathways of even small protonated heterocyclic molecules are not well characterized. The elimination of CO from furanH$^+$ is the only fragmentation process observed upon IRMPD under the present experimental conditions. Two major classes of mechanisms appear to be feasible and they are investigated and discussed in more detail for isomer **2**. The first type (A) involves a 1,2 H shift followed by ring opening and subsequent CO dissociation, whereas in the second type (B) the ring opening precedes the 1,2 H shift. Following mechanism A, a 1,2 shift of the olefinic H_5 atom of the nonprotonated C_5 atom of **2** toward the neighboring C_4 atom is required to create a CO moiety ready for elimination. The activation barrier for this shift in **2** is calculated to be rather high (439 kJ/mol), because the corresponding intermediate can be formulated either as a carbenoid or as a biradical species with high energy content. Any other possible H_α shift in **1** or **3** will also result in a species with these characteristics, which altogether renders mechanism A unlikely to occur. Mechanism B starts with ring opening by breaking one of the C–C or C–O bonds. Calculations demonstrate that only those compounds resulting from ring opening of **1**–**3** can realistically appear as intermediates that do not possess carbenoid character. Cleavage of the C_3–C_4 bond in **1**–**3** is not considered because it leads to an open-chain product, which necessarily has to undergo a number of further substantial rearrangements before CO can be eliminated. Cleavage of either the C_2–C_3 or the C_4–C_5 bond in **2** results in carbenoid or diradical compounds, which are calculated to possess a similarly high energy content as the product of the H_5 shift in **2** (in mechanism A). Only cleavage of the O–C_2 bond in **2** leads to a relatively stable intermediate, whereas rupture of the O–C_5 bond results in energetically unfavorable species. Fig. 3 illustrates the dissociation pathway with the lowest barrier found in the present work (see supplementary material for details of the stationary points). Ring opening of **2** requires 184 kJ/mol to give an open-chain product **4** (H_2C–CH–CH–CHO^+). In accord with Hammond's postulate, the transition state closely resembles **4**, and the barrier for the reverse reaction is only 1 kJ/mol. The positive charge is delocalized in the π system of the H_2C–CH–CH moiety, and the formyl group is rotated out of the plane of the molecule in order to avoid allylic strain. In a second step, a shift of the former H_5 atom involving a barrier of 36 kJ/mol leads to **5**, which is best described as a strongly bound complex of the allyl cation and CO (H_2C–CH–CH_2^+–CO) with a dissociation energy of 95 kJ/mol. Hence, the overall barrier for dissociation of **2** into $C_3H_5^+$ and CO requires 220 kJ/mol, which corresponds to approximately 13 IR photons with 1400 cm^{-1}.

3.3. PyrroleH$^+$

Similar to furan, pyrrole is a planar heterocyclic aromatic molecule (C_{2v}) offering three nonequivalent protonation sites. Protonation can occur at C_α and C_β (**7**, **8**) as well as at N (**6**). Their structures are compared in Fig. 1, and their relative energies as well as other relevant parts of the PES of pyrroleH$^+$ are displayed in Fig. 3. In agreement with previous theoretical studies [22,24,26,27], the relative energies increase in the order **7** < **8** < **6** (0 < 22 < 87 kJ/mol). The proton affinities of 881, 859, and 794 kJ/mol are close to values derived at the G3 level (874, 855, and 797 kJ/mol) [25]. The proton affinity calculated for C_α protonation, 881 kJ/mol, is in fair agreement with the recommended experimental value of 875 kJ/mol [4]. The predicted difference in the proton affinities for C_α and C_β protonation, 22 kJ/mol, is smaller than for the case of furanH$^+$, in line with the experimental value, 6 ± 6 kJ/mol [20]. The barriers for interconversion between the three minimum structures are again large, suggesting that they could all be produced in noticeable abundances [32,35]. The PES in Fig. 3 also shows that protonation of pyrrole at all three protonation sites is an exothermic process using CH_5^+ and/or $C_2H_5^+$ as protonating agent. In fact, protonation of pyrrole at both C atoms has been inferred for protonation with $C_4H_9^+$ and NH_4^+ in a neutralization–reionization mass spectrometric study [22]. Similar to furanH$^+$, C_β protonation of pyrrole was predominantly observed in a radiolytic study using protonation with $^3He^3H^+$ [21].

Comparison of the structural parameters of pyrrole and the various pyrroleH$^+$ isomers (Fig. 1) emphasizes again the

significant effects of protonation on the geometry of the heterocyclic molecule [22,26,27]. In analogy to furan, C_α protonation (at C_2) induces large elongations of the C_2–N, C_2–C_3, and C_4–C_5 bonds, and concurrent contractions of the C_3–C_4 and C_5–N bonds. Fig. 4 compares the linear IR absorption spectra calculated for the three considered pyrroleH$^+$ isomers in the fingerprint range (900–1800 cm^{-1}). The IR spectra of all three isomers are clearly very different in this spectral range, indicating that they can readily be distinguished by IR spectroscopy. Comparison of the theoretical spectra with the measured one suggests the most stable C_α protonated pyrroleH$^+$ isomer (**7**) to be the carrier of the features in the IRMPD spectrum (Fig. 4). The most intense transitions predicted for the other two isomers (**6**, **8**) in the investigated spectral range are absent in the experimental spectrum. The IRMPD spectrum exhibits a broad and intense transition with a maximum at 1426 cm^{-1}, a width of 50 cm^{-1} and a parent depletion efficiency of 17%. Motivated by the comparison to the theoretical spectrum of **7**, the IRMPD feature is deconvoluted into three components centered at 1372, 1426, and 1470 ± 11 cm^{-1} with a width of 50 cm^{-1} and relative weights of 1.0, 3.4, and 0.1 ± 0.05. Only the calculated IR spectrum of C_α protonated pyrroleH$^+$ (**7**) can account for the observed feature. The two high-frequency components at 1426 and 1470 cm^{-1} are attributed to the two overlapping fundamentals of **7** predicted to occur at 1457 cm^{-1} (94 km/mol) and 1495 cm^{-1} (40 km/mol). The 1495 cm^{-1} mode corresponds mainly to a symmetric stretch of the C_3–C_4 and C_5–N bonds, whereas the 1457 cm^{-1} vibration is dominated by the in-plane N–H bend motion (Fig. 5). The 1372 cm^{-1} shoulder is assigned to the scissoring motion of the aliphatic CH_2 group, which compares well with the calculated frequency of 1369 cm^{-1} (45 km/mol). Weaker peaks predicted in the linear IR absorption spectrum of **7** are not present in the IRMPD spectrum due to their low IR oscillator strengths (<25 km/mol). The predicted IR spectra of C_β (**8**) and N (**6**) protonated pyrroleH$^+$ feature absorptions near 1303 cm^{-1} (48 km/mol) and 1224 cm^{-1} (61 km/mol), respectively, which are clearly absent in the experimental IRMPD spectrum. As these intensities are close to the limit for IRMPD detection, it is unclear at present whether **6** and/or **8** could have escaped spectroscopic detection due to inefficient IR multiphoton absorption or whether they are of low concentration in the assayed pyrroleH$^+$ sample. Similar to furanH$^+$, the exclusive observation of C_α protonated pyrroleH$^+$ (**7**) may also be rationalized by exothermic proton transfer from the higher-energy pyrroleH$^+$ isomers **6** and **8** to neutral pyrrole to yield **7**.

[HNC] elimination is the only fragmentation process observed upon IRMPD of pyrroleH$^+$. In analogy to CO loss of furanH$^+$ (Fig. 3), the proposed fragmentation path for [HNC] elimination of pyrroleH$^+$ (**7**) corresponds to initial ring opening by rupture of the N–C_2 bond (barrier of 270 kJ/mol) leading to **9** (H_2C–CH–CH–CHNH$^+$). This step is followed by a shift of the former H_5 atom (barrier of 67 kJ/mol) leading to **10**, a strongly bound complex of the allyl cation with HNC (dissociation energy of 218 kJ/mol). The overall reaction requires 349 kJ/mol, which corresponds to 21 IR photons with 1400 cm^{-1}. Hence, HNC elimination of pyrroleH$^+$ is much more endothermic than CO elimination of furanH$^+$, which is consistent with the significantly lower IRMPD efficiency of the former molecule (17% versus 45%) under otherwise comparable conditions.

3.4. Furan$^+$

The structure and the vibrational properties of furan in its planar neutral ground electronic state ($^1A_1$, C_{2v}) are well characterized by microwave and IR spectroscopy [54,57]. A plethora of low-resolution photoelectron spectroscopic studies have established that the ground electronic state of the planar furan radical cation ($^2A_2$) results from removal of a π electron out of the highest occupied molecular orbital, which is of a_2 symmetry [58–63]. From the analysis of the vibrational substructure of the first photoelectron band, the frequencies of three vibrational modes in the $^2A_2$ state of furan$^+$ have been determined as 104, 133, and 176 meV (839, 1073, and 1420 cm^{-1}) [59,60]. Their assignments have been confirmed by theoretical calculations, taking into account Franck–Condon factors and vibronic coupling [64–67].

The energetics and dynamics of the (photo)dissociation process of furan$^+$ have also been investigated by various mass spectrometric and spectroscopic techniques, including charge exchange [68], resonance-enhanced multiphoton ionization [69,70], photoionization [59,63], photoelectron–photoion coincidence [71,72], and fixed frequency IRMPD using a CO_2 laser [73]. The main result from this work is the existence of three relevant low-lying dissociation channels of furan$^+$, leading to $C_3H_4^+$ (CO loss), $C_2H_2O^+$ (C_2H_2 loss), and $C_3H_3^+$ ([HCO] loss), with appearance energies of 2.72 < 2.92 < 3.22 eV as measured by photoionization [71]. The measured appearance energy for CO elimination (2.72 eV, 262 kJ/mol) is close to the thermochemical threshold for the generation of propyne$^+$ (2.61 eV, 252 kJ/mol) but significantly higher than the one for allene$^+$ (2.00 eV, 193 kJ/mol) [71]. As the mechanism for CO elimination is complex [63,74], the structure of the generated $C_3H_4^+$ ion is unclear at present, although the lower-energy allene$^+$ has been favored from both experimental and theoretical arguments [63,71]. Preliminary investigations of the potential energy surface suggest that CO elimination involves in both cases initial hydrogen migration followed by C–C bond fission, with slightly lower barriers for the production of allene$^+$ [63]. The appearance energy for C_2H_2 loss (2.92 eV, 282 kJ/mol) is merely 0.2 eV (19 kJ/mol) higher than the one for CO loss [71], and calculations suggest that the product ion is ketene$^+$, generated by a dissociation path similar to the one leading to allene$^+$ [63]. In contrast, the appearance energy for [HCO] loss (3.22 eV, 311 kJ/mol), most likely leading to cyclopropenyl$^+$ rather than propargyl$^+$, is substantially higher than for CO elimination (by 0.5 eV, 48 kJ/mol) [71]. Interestingly, although these three fragmentation channels are relatively close in energy, the recent IRMPD study of furan$^+$ using a high power CO_2 laser (1000 mW) with $h\nu = 0.13$ eV ($\nu = 1025$ cm^{-1}) demonstrates the predominant production of $C_3H_4^+$, which corresponds to the lowest-energy fragment channel [73]. Almost no signal was detected in the C_2H_2 loss channel, although this process requires just the absorption of one or two more IR photon(s) [71,73]. This behaviour was rationalized by modeling of the IRMPD process at typical experimental condi-

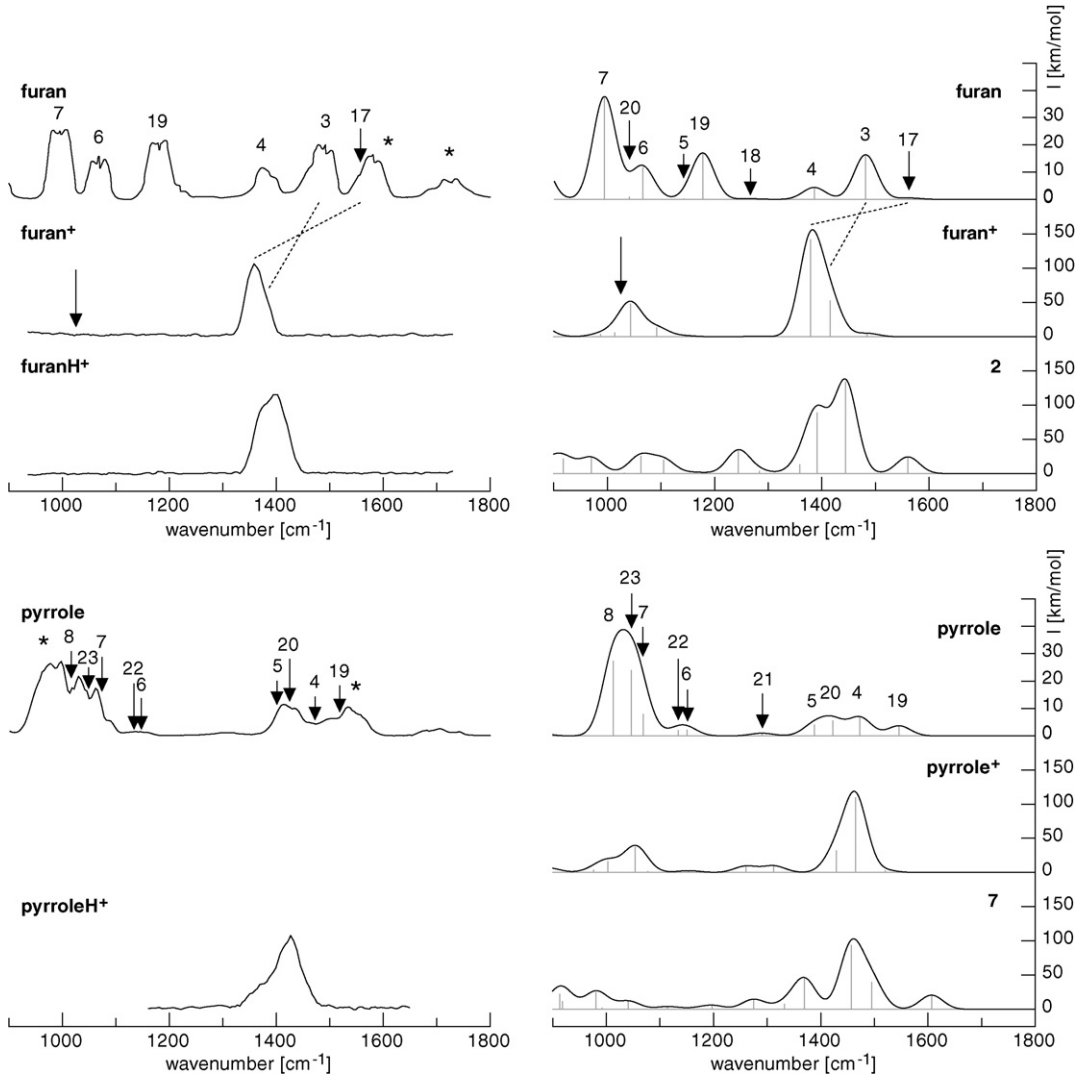

Fig. 6. Linear IR absorption spectra of furan, furan$^+$, furanH$^+$ (**2**), pyrrole, pyrrole$^+$, and pyrroleH$^+$ (**7**) calculated at the B3LYP/6-311G(2df, 2pd) level of theory (scaling factor of 0.979, convolution width of 50 cm^{-1}) are compared to the IR absorption spectra of furan and pyrrole (taken from Ref. [81]) and IRMPD spectra (R) of furan$^+$, furanH$^+$, and pyrroleH$^+$. The vibrational assignments for the neutral molecules are taken from Ref. [54]. Asterisks indicate assignments to overtones, combination bands and hot bands in the experimental IR spectra, which are not included in the theoretical spectra. The arrows in the furan$^+$ spectra indicate the position of the CO_2 laser frequency used in Ref. [73] for IRMPD ($\nu = 1025$ cm^{-1}).

tions, with the main result that the ion undergoes fragmentation, as soon as it has absorbed enough IR photons (>20) required for reaching the lowest limit for dissociation [73]. Under these apparently slow heating conditions, the dissociation rate is faster than the rate of photon absorption.

Fig. 2 shows the IRMPD signals of the furan$^+$ radical cation recorded in the three lowest-energy fragment channels. No other laser-induced fragment ions are observed upon IRMPD under the present experimental conditions. The spectral depletion observed in the parent ion signal shows good correspondence with the appearance signals in all three fragment ion channels, although the fragmentation branching ratios are strongly in favor of the lowest dissociation channel ($C_3H_4^+$). In the investigated 900–1700 cm^{-1} range, the IRMPD spectrum (Fig. 4) displays a single feature with a maximum at 1363 cm^{-1}, a width of 43 cm^{-1}, and a depletion efficiency of 32%. Deconvolution of the feature into two components using a convolution width of 31 cm^{-1} yields two transitions centered at 1354 and 1377 cm^{-1} with relative weights of 1.8:1. In general, the observed IRMPD spectrum is consistent with the linear IR absorption spectrum predicted for furan$^+$. Comparison between both spectra suggests an assignment of the more intense 1354 cm^{-1} component of the IRMPD feature to the asymmetric stretch of the C_2–C_3 and C_4–C_5 bonds, $\nu_{17}(b_2)$, calculated at 1379 cm^{-1} (143 km/mol), whereas the less intense component giving rise to the high-frequency shoulder of the IRMPD feature is attributed to the corresponding symmetric stretch, $\nu_3(a_1)$, predicted to occur at 1415 cm^{-1} (53 km/mol). Less intense transitions in the calculated furan$^+$ spectrum, such as the feature at 1043 cm^{-1} (48 km/mol), are not observed in the IRMPD spectrum, because of low IRMPD efficiency ($I < 50$ km/mol). Interestingly, the frequency of $\nu_3(a_1)$ extracted from the IRMPD spectrum (1377 cm^{-1}) is significantly lower than the one derived from He(I) photoelectron spectroscopy (1420 cm^{-1}) [60]. It is

unclear whether this discrepancy results from the low resolution of the photoelectron spectrum or from a frequency red shift arising from the subtle details of the IRMPD process. Previous IRMPD studies of molecules featuring two close-lying IR absorptions, like in the case here for furan$^+$, demonstrated that the multiphotonic character of IRMPD affects both the position and relative intensity of the two transitions [56,75–78]. An alternative explanation might be that the $\nu_3(a_1)$ mode is in fact not observed in the IRMPD spectrum due to low IR intensity (53 km/mol) and that the shoulder of the 1354 cm^{-1} band arises from an asymmetric IRMPD profile of the $\nu_{17}(b_2)$ alone.

It is interesting to compare the structures and IR spectra of furan, furan$^+$, and furanH$^+$ in order to derive the changes in the chemical bond properties upon both ionization and protonation (Figs. 1 and 6). As a general trend, the IR spectra of all three species in their ground electronic states are rather different in appearance with respect to both frequencies and IR intensities. The same is true for the corresponding pyrrole species. Removal of a single bonding π electron out of the a_2 orbital of furan weakens the C_2–C_3 and C_4–C_5 bonds. This observation is consistent with the shape of the a_2 molecular orbital, featuring a node in the symmetry plane bisecting the C_3–C_4 bonds and no nodes along the C_2–C_3 and C_4–C_5 bonds. As a result, the C_2–C_3 and C_4–C_5 bonds elongate considerably on ionization (Fig. 1), and the frequencies of the symmetric and antisymmetric stretches of both C–C bonds are reduced from $\nu_3(a_1) = 1481$ to 1415 cm^{-1} and from $\nu_{17}(b_2) = 1563$ to 1379 cm^{-1}, respectively [54]. In addition, the B3LYP calculations predict a switch in the order of the frequency and IR intensity of $\nu_3(a_1)$ and $\nu_{17}(b_2)$, indicating the substantial influence of ionization out of the a_2 orbital on the coupling between the two C–C stretch modes. All these theoretical predictions are fully consistent with the experimental IR spectra. Protonation at any of the C atoms has a rather dramatic effect on the geometry and on the vibrational mode structure in the fingerprint range. Thus, although the IRMPD spectra of furan$^+$ and furanH$^+$ look similar, the type of vibrations giving rise to the strong IR absorptions are rather different. For example, in contrast to furan$^+$, the IRMPD spectrum of furanH$^+$ features the CH_2 scissoring mode, which is characteristic of the C protonated species and frequently observed as strongly IR-active mode in IRMPD spectra of protonated aromatic molecules (AH$^+$). The frequencies of the scissoring mode can strongly vary as a function of AH$^+$, with values of 1374 cm^{-1} (furanH$^+$), 1372 cm^{-1} (pyrroleH$^+$), 1225 cm^{-1} (benzeneH$^+$) [41,43], 1260 cm^{-1} (fluorobenzeneH$^+$) [43], and 1252 cm^{-1} (tolueneH$^+$) [44]. It appears that the scissoring frequency is slightly higher for the five-membered heterocyclic molecules than for the six-membered benzene derivatives. This observation is mainly attributed to different degrees of local mode mixing with in-plane ring vibrations occurring in the same frequency range and possessing the same symmetry (Fig. 5).

In a previous study, Wu and Stace employed IRMPD of furan$^+$ to investigate experimentally and theoretically the competition between the different decomposition channels [73]. In this study, a CO_2 laser was employed with a fixed frequency of $\nu = 1025$ cm^{-1}, a typical average power of around 1000 mW and an irradiation time of the order of 1 s. The main dissociation channel observed under these relatively slow heating conditions of the molecule corresponded to CO elimination, whereas the higher lying dissociation channels were largely suppressed. For example, almost no C_2H_2 loss could be detected, although the appearance threshold for this channel is only 0.2 eV higher than the one for CO loss, that is C_2H_2 elimination requires one to two photons more than CO elimination (23 photons [71]). From this result, the authors concluded that under their conditions stepwise photoexcitation leads to prompt fragmentation once the threshold for dissociation into the lowest-energy channel is exceeded. In contrast to this previous IRMPD study using a fixed frequency CO_2 laser, the present study employs a tuneable FEL laser with similar average power (1 W) but rather different peak power arising from different pulse sequences. This change in radiation source has the following important consequences. First, as can be seen from the calculated spectrum in Fig. 6, furan$^+$ has no strong IR-active resonance at the CO_2 laser frequency (1025 cm^{-1}, marked by an arrow), i.e., the IRMPD process in Ref. [73] largely relies on nonresonant or only near resonant processes. Interestingly, no IRMPD could be detected in the present FEL study at 1025 cm^{-1}, although similar average IR laser power and 5–10 times longer irradiation times have been used. This observation is attributed to significantly less efficient overlap between the ion cloud in the MICRA cell and the FEL laser beam as compared to the previous study using an ion trap and a CO_2 laser [73]. Previous IRMPD studies on the same molecular ion using the CLIO FEL and two different ion traps, namely the FT-ICR MICRA and a Paul-type ion trap, indeed confirm that the overlap of the FEL with the ion cloud in MICRA is less optimal leading to reduced IRMPD efficiencies [52]. Second, the structure of the FEL pulses at CLIO appears to heat the molecule faster than the CO_2 laser, because resonant absorption of furan$^+$ near the strongly IR-active modes $\nu_{3/17}$ at around 1370 cm^{-1} allowed for the significant detection of the higher-energy C_2H_2 (5%) and [HCO] loss (3%) channels, in addition to the predominant CO loss channel (92%). Hence, comparison of both IRMPD studies clearly demonstrates that the branching ratios for competing dissociation channels strongly depend on the time structure of the IR laser source, and not only on the average IR power. Moreover, the branching ratios may also sensitively depend on the IR laser frequency. While slow nonresonant heating using the CO_2 laser may strongly favor the lowest-energy fragment channel [73], fast resonant heating using the FEL increases the probability to promote dissociation into higher lying fragmentation channels [78]. This is in line with the recent observations made in an IRMPD study of the protonated dimers of simple alcohols, where two reaction channels with different barriers are competing [79].

3.5. Dissociation energies and IRMPD yields

According to Ref. [71] and the present calculations, the appearance energies for photofragmentation rise in the order furanH$^+$ < furan$^+$ < pyrroleH$^+$ (219 < 262 < 349 kJ/mol), which correspond to the absorption of around 13 < 16 < 21 photons with 1400 cm^{-1}. This result is consistent with the decreasing

efficiency (45 > 32 > 17%) observed for resonant IRMPD near 1400 cm^{-1} for transitions with comparable IR oscillator strengths.

In contrast to furan$^+$, furanH$^+$, and pyrroleH$^+$, efforts in recording IRMPD spectra of the related heterocyclic molecules pyrrole$^+$, imidazoleH$^+$, and pyridineH$^+$ were unsuccessful under similar experimental conditions, despite the application of relatively high laser intensities (∼1 W) and relatively long irradiation times (∼10 s). The failure cannot be attributed to insufficient ion concentrations, as all ions could be produced with similar yields by chemical ionization in the ICR cell. As the IR-active modes of N protonated pyridineH$^+$ and imidazoleH$^+$ have calculated oscillator strengths below 50 km/mol in the investigated spectral range [40], these ions may simply not fragment due to inefficient multiphoton absorption. In contrast, pyrrole$^+$ possesses sufficiently strong absorptions to be detectable with IRMPD in the investigated spectral range, with intensities larger than 100 km/mol (Fig. 6). Hence, the failure for observation of IRMPD of pyrrole$^+$ must arise either from slow intramolecular vibrational energy redistribution rates and/or its large binding energy (331 kJ/mol [80]). Both reasons may also apply to imidazoleH$^+$ and pyridineH$^+$. N containing heterocyclic ions have usually large thermodynamic thresholds for dissociation, as the lowest dissociation channel often involves the elimination of the relatively unstable HNC molecule [81,82]. In this context, it is interesting to note that several attempts to record an IRMPD spectrum of benzene$^+$ have failed [41], whereas IRMPD spectra could readily be obtained for a large variety of larger polycyclic aromatic hydrocarbon radical cations (PAH$^+$) [42,77]. Consequently, the IR spectrum of benzene$^+$ could so far only be inferred from IRPD of weakly bound $C_6H_6{}^+$–L_n clusters [83–90].

4. Conclusions

For the first time, the protonation sites of the fundamental heterocyclic aromatic molecules furan and pyrrole have been characterized in the gas phase by spectroscopic tools. Protonated furan and pyrrole have been generated by chemical ionization using $CH_5{}^+$ and/or $C_2H_5{}^+$ in a FT-ICR mass spectrometer and characterized by IRMPD spectroscopy in the fingerprint range using the FEL at CLIO. Comparison with B3LYP/6-311G(2df, 2pd) calculations demonstrates unambiguously that only the C_α protonated isomers are observed, which correspond to the global minima on the PES of both protonated heterocyclic molecules. No signatures of the less stable isomers corresponding to protonation at the C_β atom or the heteroatom are detected. The IRMPD spectrum of the furan radical cation has been detected as well. Comparison of the IR spectra of the neutral molecules with the IRMPD spectra of the radical cation and the protonated species are consistent with the geometrical changes predicted for ionization out of the a_2 orbital and protonation at C_α, respectively. Future experiments aim at the investigation of isolated and microsolvated furanH$^+$ and pyrroleH$^+$ ions in the X–H stretch region (X = C, O, N) by IRPD spectroscopy [91–93] in order to characterize both the less stable C_β and O/N protonated isomers (generated in a supersonic plasma expansion) and the effects of stepwise solvation on the properties of the protonation process of these fundamental heterocyclic molecules [29–40].

Supporting information

The supporting information supplies energetic, structural and vibrational data of relevant stationary points on the PES of furan, pyrrole, furan(H)$^+$ and pyrrole(H)$^+$.

Acknowledgements

This work was supported by the CNRS, the University of Paris-Sud and especially its laser facility POLA, the Italian MIUR, and the *Deutsche Forschungsgemeinschaft* (DO 729/2). We thank Jean-Michel Ortega and his coworkers at the CLIO facility for their support during the experiments. Financial support by the European Commission (project IC 002-05) is gratefully acknowledged (travel grants to M.E.C. and O.D.). Financial support by the European Commission through the NEST/ADVENTURE program (EPITOPES, project #15637) is also gratefully acknowledged (J.L. and P.M.).

Appendix A. Supplementary data

Supplementary data associated with this article can be found, in the online version, at doi:10.1016/j.ijms.2007.02.017.

References

[1] R. Stewart, The Proton: Applications to Organic Chemistry, Academic Press, New York, 1985.
[2] M.B. Smith, J. March, Advanced Organic Chemistry: Reactions, Mechanisms, and Structure, Wiley, New York, 2001.
[3] L. Stryer, Biochemistry, Freeman, New York, 1996.
[4] E.P.L. Hunter, S.G. Lias, J. Phys. Chem. Ref. Data 27 (1998) 413.
[5] D. Kuck, Mass Spectrom. Rev. 9 (1990) 583.
[6] G.A. Olah, Acc. Chem. Res. 4 (1971) 240.
[7] V.A. Koptyug, Top. Curr. Chem. 122 (1984) 1.
[8] R.J. Sundberg, R.B. Martin, Chem. Rev. 74 (1974) 471.
[9] A.T. Balaban, D.C. Oniciu, A.R. Katritzky, Chem. Rev. 104 (2004) 2777.
[10] B.H. Lipshutz, Chem. Rev. 86 (1986) 795.
[11] G. Marino, Adv. Heterocycl. Chem. 13 (1971) 235.
[12] A. Streitwieser, Organische Chemie, VCH, Basel, 1994.
[13] M. Salmon, K.K. Kanazawa, A.F. Diaz, M. Krounbi, J. Polym. Sci. Part C: Polym. Lett. 20 (1982) 187.
[14] R.Y. Qian, Q.B. Pei, Z.T. Huang, Macromol. Chem. Phys. 192 (1991) 1263.
[15] Y. Chiang, E.B. Whipple, J. Am. Chem. Soc. 85 (1963) 2763.
[16] D.M. Muir, M.C. Whiting, J. Chem. Soc.: Perkin Trans. 2 (1976) 388.
[17] D.M. Muir, M.C. Whiting, J. Chem. Soc.: Perkin Trans. 2 (1975) 1316.
[18] G.P. Bean, T.J. Wilkinson, J. Chem. Soc.: Perkin Trans. 2 (1978) 72.
[19] R. Houriet, H. Schwarz, W. Zummack, Angew. Chem. Int. Ed. 19 (1980) 905.
[20] R. Houriet, H. Schwarz, W. Zummack, J.G. Andrade, P.V.R. Schleyer, New J. Chem. 5 (1981) 505.
[21] G. Angelini, G. Laguzzi, C. Sparapani, M. Speranza, J. Am. Chem. Soc. 106 (1984) 37.
[22] V.Q. Nguyen, F. Turecek, J. Mass. Spectrom. 31 (1996) 1173.
[23] E.S.E. van Beelen, T.A. Koblenz, S. Ingemann, S. Hammerum, J. Phys. Chem. A 108 (2004) 2787.
[24] M. Esseffar, E. Quintanilla, J.Z. Davalos, J.L.M. Abboud, O. Mo, M. Yanez, New J. Chem. 26 (2002) 1567.

[25] S. Kabli, E.S.E. van Beelen, S. Ingemann, L. Henriksen, S. Hammerum, Int. J. Mass Spectrom. 249 (2006) 370.
[26] K. Zeng, Z.X. Cao, Chin. J. Chem. 24 (2006) 293.
[27] L.I. Belenkii, I.A. Suslov, D.D. Chuvylkin, Chem. Heterocycl. Compd. 39 (2003) 36.
[28] O. Dopfer, J. Phys. Org. Chem. 19 (2006) 540.
[29] N. Solcà, O. Dopfer, Angew. Chem. Int. Ed. 41 (2002) 3628.
[30] N. Solcà, O. Dopfer, Chem. Eur. J. 9 (2003) 3154.
[31] C. Chaudhuri, C.-C. Wu, J.-C. Jiang, H.-C. Chang, Aus. J. Chem. 57 (2004) 1153.
[32] N. Solcà, O. Dopfer, J. Am. Chem. Soc. 125 (2003) 1421.
[33] N. Solcà, O. Dopfer, Angew. Chem. Int. Ed. 42 (2003) 1537.
[34] N. Solcà, O. Dopfer, Chem. Phys. Lett. 342 (2001) 191.
[35] N. Solcà, O. Dopfer, J. Am. Chem. Soc. 126 (2004) 1716.
[36] N. Solcà, O. Dopfer, J. Chem. Phys. 120 (2004) 10470.
[37] N. Solcà, O. Dopfer, J. Chem. Phys. 121 (2004) 769.
[38] N. Solcà, O. Dopfer, Chem. Phys. Chem. 6 (2005) 434.
[39] F. Pasker, N. Solcà, O. Dopfer, J. Phys. Chem. A 110 (2006) 12793.
[40] H.S. Andrei, N. Solcà, O. Dopfer, Chem. Phys. Chem. 7 (2006) 107.
[41] W. Jones, P. Boissel, B. Chiavarino, M.E. Crestoni, S. Fornarini, J. Lemaire, P. Maitre, Angew. Chem. Int. Ed. 42 (2003) 2057.
[42] J. Oomens, B.G. Sartakov, G. Meijer, G. von Helden, Int. J. Mass Spectrom. 254 (2006) 1.
[43] O. Dopfer, N. Solcà, J. Lemaire, P. Maitre, M.E. Crestoni, S. Fornarini, J. Phys. Chem. A 109 (2005) 7881.
[44] O. Dopfer, J. Lemaire, P. Maitre, M.E. Crestoni, S. Fornarini, Int. J. Mass Spectrom. 249–250 (2006) 149.
[45] D. Schröder, H. Schwarz, P. Milko, J. Roithova, J. Phys. Chem. A 110 (2006) 8346.
[46] J. Oomens, G. von Helden, G. Meijer, Int. J. Mass Spectrom. 249–250 (2006) 199.
[47] B. Chiavarino, M.E. Crestoni, S. Fornarini, J. Lemaire, L. MacAleese, P. Maitre, Chem. Phys. Chem. 6 (2005) 437.
[48] B. Chiavarino, M.E. Crestoni, S. Fornarini, O. Dopfer, J. Lemaire, P. Maitre, J. Phys. Chem. A 110 (2006) 9352.
[49] J. Oomens, G. von Helden, G. Meijer, J. Phys. Chem. A 108 (2004) 8273.
[50] G. Mauclaire, J. Lemaire, P. Boissel, G. Bellec, M. Heninger, Eur. J. Mass Spectrom. 10 (2004) 155.
[51] P. Maitre, S. Le Caer, A. Simon, W. Jones, J. Lemaire, H. Mestdagh, M. Heninger, G. Mauclaire, P. Boissel, R. Prazeres, F. Glotin, J.M. Ortega, Nucl. Instrum. Meth., Sect. A 507 (2003) 541.
[52] L. MacAleese, A. Simon, T.B. McMahon, J.M. Ortega, D. Scuderi, J. Lemaire, P. Maitre, Int. J. Mass Spectrom. 249–250 (2006) 14.
[53] M.J. Frisch, G.W. Trucks, H.B. Schlegel, G.E. Scuseria, M.A. Robb, J.R. Cheeseman, J.A. Montgomery, T. Vreven, K.N. Kudin, J.C. Burant, J.M. Millam, S.S. Iyengar, J. Tomasi, V. Barone, B. Menucci, M. Cossi, G. Scalmani, N. Rega, G.A. Petersson, H. Nakatsuji, M. Hada, M. Ehara, K. Toyota, R. Fukuda, J. Hasegawa, M. Ishida, T. Nakajima, Y. Honda, O. Kitao, H. Nakai, M. Klene, X. Li, J.E. Knox, H.P. Hratchian, J.B. Cross, C. Adamo, J. Jaramillo, R. Gomperts, R.E. Stratman, P.Y. Yazyev, A.J. Austin, R. Cammi, C. Pomelli, J. Ochterski, P.Y. Ayala, K. Morokuma, G.A. Voth, P. Salvador, J.J. Dannenberg, V.G. Zakrzewski, S. Dapprich, A.D. Daniels, M.C. Strain, O. Farkas, D.K. Malick, D. Rabuck, K. Raghavachari, J.B. Foresman, J.V. Ortiz, Q. Cui, A.G. Baboul, S. Clifford, J. Cioslowski, B.B. Stefanov, G. Liu, A. Liashenko, P. Piskorz, I. Komaromi, R.L. Martin, D.J. Fox, T. Keith, M.A. Al-Laham, C.Y. Peng, A. Nanayakkara, M. Challacombe, P.M.W. Gill, B.G. Johnson, W. Chen, M.W. Wong, C. Gonzales, J.A. Pople, Gaussian 03, Revision C. 02, Gaussian Inc., Pittsburgh, PA, 2004.
[54] A. Mellouki, J. Lievin, M. Herman, Chem. Phys. 271 (2001) 239.
[55] D. Heidrich, Angew. Chem. Int. Ed. 41 (2002) 3208.
[56] A. Simon, W. Jones, J.M. Ortega, P. Boissel, J. Lemaire, P. Maitre, J. Am. Chem. Soc. 126 (2004) 11666.
[57] M.H. Sirvetz, J. Chem. Phys. 19 (1951) 1609.
[58] J.A. Sell, A. Kuppermann, Chem. Phys. Lett. 61 (1979) 355.
[59] P.J. Derrick, L. Asbrink, O. Edqvist, B.O. Jonsson, E. Lindholm, Int. J. Mass Spectrom. Ion Phys. 6 (1971) 161.
[60] P.J. Derrick, L. Asbrink, O. Edqvist, E. Lindholm, Spectrochim. Acta, Part A A27 (1971) 2525.
[61] T. Munakata, K. Kuchitsu, Y. Harada, J. Electron Spectrosc. Relat. Phenom. 20 (1980) 235.
[62] L. Klasinc, A. Sabljic, G. Kluge, J. Rieger, M. Scholz, J. Chem. Soc., Perkin Trans. 2 (1982) 539.
[63] E.E. Rennie, C.A.F. Johnson, J.E. Parker, D.M.P. Holland, D.A. Shaw, M.A. MacDonald, M.A. Hayes, L.G. Shpinkova, Chem. Phys. 236 (1998) 365.
[64] W.V. Niessen, L.S. Cederbaum, G.H.F. Diercksen, J. Am. Chem. Soc. 98 (1976) 2066.
[65] K. Takeshita, Y. Yamamoto, Theor. Chim. Acta 92 (1995) 199.
[66] S. Bonness, B. Kirtman, M. Huix, A.J. Sanchez, J.M. Luis, J. Chem. Phys. 125 (2006).
[67] A.B. Trofimov, H. Koppel, J. Schirmer, J. Chem. Phys. 109 (1998) 1025.
[68] J.M. Tedder, P.H. Vidaud, J. Chem. Soc., Faraday Trans. 2 (76) (1980) 1516.
[69] C.D. Cooper, A.D. Williamson, J.C. Miller, R.N. Compton, J. Chem. Phys. 73 (1980) 1527.
[70] T. Ridley, K.P. Lawley, R.J. Donovan, Phys. Chem. Chem. Phys. 6 (2004) 5304.
[71] G.D. Willett, T. Baer, J. Am. Chem. Soc. 102 (1980) 6769.
[72] E.E. Rennie, L. Cooper, C.A.F. Johnson, J.E. Parker, R.A. Mackie, L.G. Shpinkova, D.M.P. Holland, D.A. Shaw, M.A. Hayes, Chem. Phys. 263 (2001) 149.
[73] G. Wu, A.J. Stace, Chem. Phys. Lett. 412 (2005) 1.
[74] D.M. Willberg, M. Gutmann, E.E. Nikitin, A.H. Zewail, Chem. Phys. Lett. 201 (1993) 506.
[75] C. Kapota, J. Lemaire, P. Maitre, G. Ohanessian, J. Am. Chem. Soc. 126 (2004) 1836.
[76] B. Chiavarino, M.E. Crestoni, S. Fornarini, J. Lemaire, L. Mac Aleese, P. Maitre, Chem. Phys. Chem. 5 (2004) 1679.
[77] J. Oomens, A.G.G.M. Tielens, B.G. Sartakov, G. von Helden, G. Meijer, Astrophys. J. 591 (2003) 968.
[78] J. Oomens, D.T. Moore, G. Meijer, G. von Helden, Phys. Chem. Chem. Phys. 6 (2004) 710.
[79] T.D. Fridgen, L. MacAleese, T.B. McMahon, J. Lemaire, P. Maitre, Phys. Chem. Chem. Phys. 8 (2006) 955.
[80] G.D. Willett, T. Baer, J. Am. Chem. Soc. 102 (1980) 6774.
[81] P.J. Linstrom, W.G. Mallard, NIST Chemistry WebBook, National Institute of Standards and Technology, Gaithersburg, MD, 2001, p. 20899 http://webbook.nist.gov.
[82] H.S. Andrei, N. Solcà, O. Dopfer, J. Phys. Chem. A 109 (2005) 3598.
[83] O. Dopfer, R.V. Olkhov, J.P. Maier, J. Chem. Phys. 111 (1999) 10754.
[84] R.G. Satink, H. Piest, G. von Helden, G. Meijer, J. Chem. Phys. 111 (1999) 10750.
[85] A. Fujii, E. Fujimaki, T. Ebata, N. Mikami, Chem. Phys. Lett. 303 (1999) 289.
[86] M. Miyazaki, A. Fujii, T. Ebata, N. Mikami, Chem. Phys. Lett. 349 (2001) 431.
[87] M. Miyazaki, A. Fujii, N. Mikami, J. Phys. Chem. A 108 (2004) 8269.
[88] J.M. Bakker, R.G. Satink, G. von Helden, G. Meijer, Phys. Chem. Chem. Phys. 4 (2002) 24.
[89] N. Solcà, O. Dopfer, Chem. Phys. Lett. 347 (2001) 59.
[90] N. Solcà, O. Dopfer, J. Phys. Chem. A 107 (2003) 4046.
[91] O. Dopfer, Int. Rev. Phys. Chem. 22 (2003) 437.
[92] O. Dopfer, Z. Phys. Chem. 219 (2005) 125.
[93] E.J. Bieske, O. Dopfer, Chem. Rev. 100 (2000) 3963.